Optimal Inter- and Intra-Hour Scheduling of Islanded Integrated-Energy System Considering Linepack of Gas Pipelines

Zhejing Bao, *Member, IEEE*, Dawei Chen, Lei Wu, *Senior Member, IEEE*, Xiaogang Guo

***Abstract*—In an integrated energy system (IES), such as electricity-heating-gas system, remarkable difference in response time among multiple energy subsystems make the overall energy scheduling a challenging issue. Meanwhile, storage capabilities, such as inherent storage capability of gas pipelines, provide a potential way to improve system scheduling flexibility. In this paper, an optimal scheduling approach for IES operated in an islanded mode is developed, while covering inter- and intra-hour timescales simultaneously. Specifically, in inter-hour timescale, steady-state models of individual energy subsystems are used, and the heuristic particle swarm optimization (PSO) is integrated into the decomposition-based sequential multi-energy flow (MEF) calculation to derive optimal scheduling of CHPs and flow rates of gas sources with respect to forecasts of renewable energy sources (RESs); While in intra-hour timescale, with the dynamic model of gas flows, the optimal range of pressure of gas source node is scheduled to ensure robustness against RES uncertainties while leveraging storage capabilities of gas pipelines. An integrated energy test system is studied to demonstrate effects of integrated inter-hour and intra-hour schedules in handling different dynamic response time and effects of storages capabilities of gas linepack in achieving robust operation against uncertainties.**

***Index Terms*—Integrated energy system (IES), multi-energy flow (MEF), particle swarm optimization (PSO), scheduling, uncertainty.**

NOMENCLATURE

Indices and Parameters:

λ	Friction factor of gas pipeline
d	Pipeline diameter of gas network
e	Cost coefficient
k	Weymouth constant of gas pipeline
s	Scenarios of RES power outputs during intra-hour period
t	Time in intra-hour dispatching, i.e., in seconds
$\boldsymbol{A}$	Incidence matrix of heating network
$\boldsymbol{B}$	Loop incidence matrix of heating network
CW	Specific heat capacity of water
$\boldsymbol{G}$	Incidence matrix of gas network
L	Pipeline length of gas network
$\boldsymbol{R}$	Resistance coefficient vector of each heating pipeline
S	Pipeline cross-sectional area of gas network
T	Time in inter-hour scheduling, i.e., in hours
Y	Nodal admittance matrix of electricity network

Superscripts and subscripts

in	At the end of an incoming heating pipeline
re	Return at the outlet of a node before mixing in heating network
supp	Supply at a node of heating network
out	At the start of an out-going heating pipeline
CHP	CHP unit with fixed or variable heat-to-electricity ratio
CHP_f	CHP unit with fixed heat-to-electricity ratio
CHP_v	CHP unit with variable heat-to-electricity ratio
N	Nodes in heating or gas network
P	Pipelines in heating or gas network
P_RES	Forecast on output power of RES
SD	Shutdown of a CHP unit
S_RES	Scenarios of RES power output
SU	Startup of a CHP unit

Variables:

θ	Voltage angle difference between nodes
Φ	Heat power transferred to load node via heating network
π	Gas pressure of a node in inter-hour scheduling
π'	Gas pressure of a node in intra-hour dispatching
ρ	Density of natural gas
h	Head loss of heating pipeline
m	Mass flow rate within heating network
v	Startup status of CHP unit: 1 if unit starts up and 0 otherwise
w	Shutdown status of CHP unit: 1 if unit shuts down and 0 otherwise
F	Gas fuel consumption of CHP
H	Heating power
M	Mass flow rate in gas network in inter-hour scheduling
M'	Mass flow rate in gas network in intra-hour dispatching
P	Electric active power
Q	Electric reactive power
S	Electrical apparent power
T	Water temperature in heating network
U	Voltage magnitude at bus

I. INTRODUCTION

THE integrated energy system (IES) is becoming a focus of research and application, due to the urgent needs in dealing with the increasing energy shortage and environmental pollution issues all over the world [1], [2]. In an IES, individual energy subsystems, i.e., electricity, heating, and gas infrastructures, are interconnected by energy coupling components, such as combined heat and power units (CHP), heat pumps, electric/gas boiler and so on. Meanwhile, energy travelling speeds in electricity, gas, and thermal subsystems differ in the order of several magnitudes, while they also represent distinct physical characteristics. Hence, it is imperative to implement the integrated multi-energy analysis and co-optimization for IES.

The multi-energy flow analysis and multi-energy coordinated scheduling have attracted many attentions in academic research. A convex optimization based distributed algorithm was proposed to solve multi-period optimal gas-power flow problem in coupled energy distribution system [3]. A robust security-constrained unit commitment model was studied to enhance the reliability of integrated electricity-gas IES system [4]. An interval optimization based coordinated operating strategy for the electricity-gas IES was investigated, considering demand response and wind power uncertainty [5]. The coordination of electricity and gas infrastructures for minimizing the expected operation cost was discussed in a stochastic day-ahead scheduling [6]. A hierarchical framework was established for an IES, including day-ahead scheduling and intra-hour adjustment [7]. A quasi-steady multi-energy flow model was developed to consider different system dynamics, in which a transformation technique was adopted to handle different

This work was supported by the National Natural Science Foundation of China under Grant no. 51777182, and in part supported by the U.S. National Science Foundation under Grant no. CMMI-1635339.

Z. J. Bao, D. W. Chen and X. G. Guo are with College of Electrical Engineering, Zhejiang University, Hangzhou 310027, China (e-mail: zjbao@zju.edu.cn).

L. Wu is with the ECE Department, Stevens Institute of Technology, Hoboken, NJ, 07030, USA (e-mail: lei.wu@stevens.edu).

heating network nodes [8]. The coupled and sequential interval energy flow analysis of IES with RES uncertainties was implemented [9]. Transmission-constrained unit commitment problem was solved respectively by a linear optimization and an iterative method to coordinate the short-term operation of electricity-heating IES [10, 11]. Two combined analysis methods were proposed to study the performance of electricity-heat IES [12].

Moreover, some research works have investigated the accommodation of renewable energy in IES. In [6], a scenario generation based approach was applied to describe variability of wind power, and load shedding was conducted to compensate unavailability of wind energy in electricity and natural gas coupled infrastructure. Various energy demand response resources were utilized to smooth the tie-power fluctuations flexibly in an integrated community energy system, taking into account the uncertainties associated with renewable generations and loads [13]. The utilization of customers' flexible energy demand was investigated to provide balancing resources and relieve the difficulties in integrating variable wind power with the combined heat and electricity IES [14]. The scheduling of gas-fired power generation and P2G was explored to accommodate high penetration levels of intermittent renewable energy, in which the hour based steady-state model was adopted [15].

On one hand, for multi-energy coordinated scheduling, most of the existing research focused on either gas-electricity [3-7, 13, 15-18] or heat-electricity coupled system [8, 9, 10-12, 14]. To the best of our knowledge, the coordinated scheduling for electricity-heating-gas coupled system considering multi-energy flow is very limited. Moreover, in most of the previous gas-electricity coordinated scheduling, the steady-state model of natural gas is usually considered with given approximated gas source pressure values [3-7, 13, 15-18], while the gas source pressure optimization is neglected. However, when the shorter time-scale is studied, especially intra-hour, the steady-state gas model may result in suboptimal or even infeasible scheduling coordination [19]. In addition, the coordination of two types of complementary CHPs, in terms of the fixed and variable heat-to-electricity ratios, has been seldom discussed in multi-energy coupled system, which is critical to achieve strict supply/demand balance of electricity power especially when the main grid is out of service.

On the other hand, in terms of mitigating RES uncertainties in multi-energy coupled system, most researches still focus on the traditional mitigation means, such as load shedding [6] and demand response [13, 14] that have been widely studied in individual energy network. However, the flexibility offered by distinct energy storage characteristics within the natural gas network, referred to as linepack, has been largely neglected. Although the natural gas linepack based flexibility to the operation of multi-energy coupled system has been discussed in several works [20, 21], most of them are conducted via the natural gas steady-state model, rather than the optimal operational scheduling with the natural gas dynamical model.

To fill in existing gaps, this paper proposes an integrated inter-hour and intra-hour combined multi-energy coordinated scheduling approach for islanded electricity-heating-gas IES. Specifically, in the inter-hour scheduling, the steady-state models of multi-energy subsystems together with forecasts on RES outputs are used, and a heuristic particle swarm optimization (PSO) approach is integrated with a decomposition-based sequential MEF calculation method to derive optimal scheduling of CHPs and gas flow rate of gas source node to achieve economic viability and physical feasibility. In addition, in recognizing relatively slow traveling speed of gas flows through pipelines, adjusting flow rate at source node to balance instantaneous electric energy supply and demand mismatch caused by RES forecasting errors would be physically infeasible. Therefore, an intra-hour dispatching strategy is proposed, in which an optimal range of pressure of gas source node is determined to achieve robustness of IES against RES uncertainties, by flexibly utilizing storage capacities in gas pipelines. The main contributions of this paper are twofold:

1. A comprehensive multi-energy coordinated scheduling framework for electricity-heating-gas coupled system is proposed, in which steady-state models of individual energy subsystem in inter-hour timescale and dynamical model of gas flows in intra-hour timescale are combined. Moreover, the coordination of two types of complementary CHPs, corresponding to the fixed and variable heat-to-electricity ratios, is also investigated.

2. For the multi-energy system, by utilizing operational flexibility provided by inherent energy storage capability of the natural gas network, a robust gas source pressure dispatching approach while considering gas dynamics is discussed, aiming to mitigate the fluctuation of renewable energy.

The remaining of this paper is organized as follows. Section II provides schematic overview of the two-timescale scheduling approach. Section III illustrates the inter-hour multi-energy coordinated scheduling. In Section IV, the intra-hour dispatching on pressure at gas source node is described. Section V presents simulation results, and conclusions are drawn in Section VI.

II. Schematic Overview of Two-Timescale Scheduling

Schematic overview of the two-timescale multi-energy coupled scheduling optimization of islanded IES is illustrated in Fig. 1. With the forecasts of hourly RES outputs, the inter-hour scheduling is implemented to optimize outputs of CHPs and flow rate at gas source node, aiming at minimizing operation costs while satisfying MEF constraints. Because gas flow rate through a gas pipeline is proportional to the squared pipeline pressure drop in the steady-state operation, an approximate value is set to the gas pressure at gas source node in the inter-hour scheduling as long as gas pressures of load nodes can maintain within their secure constraints.

Owing to the inherent uncertainties of RESs, the persistent prediction errors will have a significant impact on the operation of the islanded IES, in which the strict supply and demand balance of electricity power is critical. In IES, the

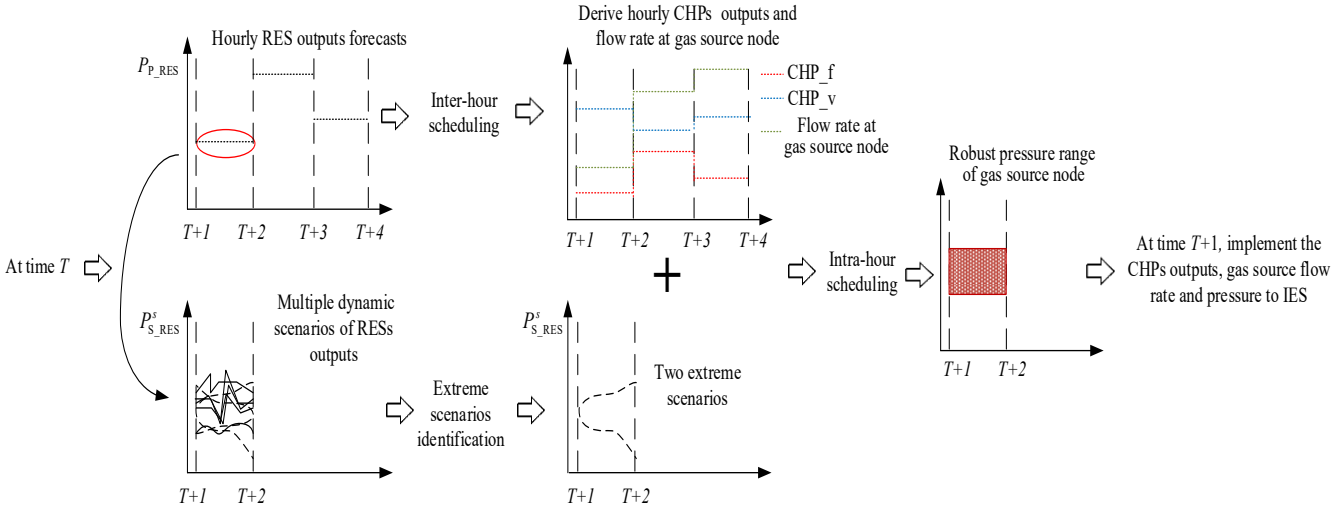

Fig. 1. Schematic overview of the two-timescale optimal scheduling of islanded IES.

flexibility provided by energy storage characteristics of natural gas infrastructure can help accommodate intermittent RESs. First of all, before intra-hour scheduling, multiple dynamic scenarios of RESs output are generated to simulate the uncertainties; and then the two extreme scenarios in terms of linepack variations are identified. With the optimal scheduling results of hourly CHPs outputs and gas flow rates of gas source nodes obtained from the inter-hour scheduling, along with the two extreme scenarios, the intra-hour scheduling strategy is further conducted to determine the robust pressure range of gas source nodes against uncertainties and variabilities of RESs, with which the prediction error of RES forecasting can be effectively handled. CHP units with variable heat-to-electricity ratios serve as slack nodes, which are used to mitigate the discrepancy between the predicted and actual RES outputs.

At time T, the inter- and intra-hour coordinated scheduling of IES considering linepack of gas pipelines is carried out; and then at the following time T+1, the obtained scheduling results of CHPs outputs as well as mass flow rates and pressures at gas source nodes are implemented to the IES.

III. Inter-Hour Multi-Energy Coordinated Scheduling

In an islanded IES, two types of CHPs with complementary properties are considered. One type uses gas turbine or internal combustion reciprocating engine with a fixed heat-to-electricity ratio, and the other uses extraction steam turbines which can be operated within a wide range of heat-to-electricity ratio. Usually, owing to the fixed heat-to-electricity ratio, the former usually has higher energy conversion efficiency than the latter. The effective coordination of the two types of complementary CHPs make it possible to simultaneously meet electricity and heat demands.

Specifically, in an islanded IES, CHPs and RESs supply electricity energy via electricity grid, CHPs satisfy heating demand through heating network, and gas source is used to meet electricity generation and non-generation gas demands through gas network. Considering hourly time resolution in the inter-hour scheduling, the steady-state models of energy coupling components, electricity network, hydraulic-thermal network, and gas network are applied.

A. Objective

The objective of the inter-hour scheduling problem is to minimize the operation cost as shown in (1), i.e., the cost of natural gas for satisfying gas demands from CHPs as well as their startup and shutdown costs. In the proposed model, the cost of non-generation gas demands is constant with no influence on the scheduling of CHPs coordination and excluded from (1), by assuming that those loads are fixed and should be satisfied without shedding. That is, (1) only includes the total cost for satisfying electricity loads, CHP gas loads, and thermal demands. In (1), cost coefficient e_{GAS} is measured in Yuan/MWh, $e^{\mathrm{SU}}_{\mathrm{CHP}}$ and $e^{\mathrm{SD}}_{\mathrm{CHP}}$ are measured in Yuan.

$$\begin{aligned}\min\ & e_{\mathrm{GAS}} \sum_{T=1}^{Inter-T}\left(F_{\mathrm{CHP\_v}}(T)+F_{\mathrm{CHP\_f}}(T)\right)\\ &+e^{\mathrm{SU}}_{\mathrm{CHP}} \sum_{T=1}^{Inter-T}\left(v_{\mathrm{CHP\_v}}(T)+v_{\mathrm{CHP\_f}}(T)\right)\\ &+e^{\mathrm{SD}}_{\mathrm{CHP}} \sum_{T=1}^{Inter-T}\left(w_{\mathrm{CHP\_v}}(T)+w_{\mathrm{CHP\_f}}(T)\right)\end{aligned} \tag{1}$$

B. Operation Constraints

- *Constraints of Energy Coupling Components*

As an important energy coupling component, CHPs generate electricity and heat energy while consuming natural gas. Two complementary types of CHPs are considered, which operate in a coordinated way to meet electricity and heat demands.

The first type of CHP uses gas turbine or internal combustion reciprocating engine with a fixed heat-to-electricity ratio, which can be modeled as in (2)-(4) where the parameters $c_{\mathrm{CHP\_f}}$ and $a_{\mathrm{CHP\_f}}$ are considered constant.

$$H_{\mathrm{CHP\_f}}(T)=c_{\mathrm{CHP\_f}}P_{\mathrm{CHP\_f}}(T) \tag{2}$$

$$F_{\mathrm{CHP\_f}}(T)=a_{\mathrm{CHP\_f}}P_{\mathrm{CHP\_f}}(T) \tag{3}$$

$$0\le P_{\mathrm{CHP\_f}}(T)\le \overline{P_{\mathrm{CHP\_f}}} \tag{4}$$

The second type of CHP uses extraction steam turbines that can be operated within a wide range of heat-to-electricity ratio. In (5)-(6), the feasible operation region of the CHP is described by a polygon via four lines as shown in Fig. 2,

where the lines with slope $c_{\mathrm{CHP\_v1}}$ and $-c_{\mathrm{CHP\_v2}}$ ($c_{\mathrm{CHP\_v2}}>0$) respectively define the lower and upper limits of electric power output with respect to any level of heat power output. For the electricity power generation $P_{\mathrm{CHP\_v}}(T)$ and the by-product heat power generation $H_{\mathrm{CHP\_v}}(T)$, the gas consumption by CHP unit is calculated as in (7).

$$0 \le H_{\mathrm{CHP\_v}}(T) \le \overline{H_{\mathrm{CHP\_v}}} \tag{5}$$

$$c_{\mathrm{CHP\_v1}} H_{\mathrm{CHP\_v}}(T) \le P_{\mathrm{CHP\_v}}(T) \le \overline{P_{\mathrm{CHP\_v}}} - c_{\mathrm{CHP\_v2}} H_{\mathrm{CHP\_v}}(T) \tag{6}$$

$$F_{\mathrm{CHP\_v}}(T) = a_{\mathrm{CHP\_v}} H_{\mathrm{CHP\_v}}(T) + b_{\mathrm{CHP\_v}} P_{\mathrm{CHP\_v}}(T) + g_{\mathrm{CHP\_v}} \tag{7}$$

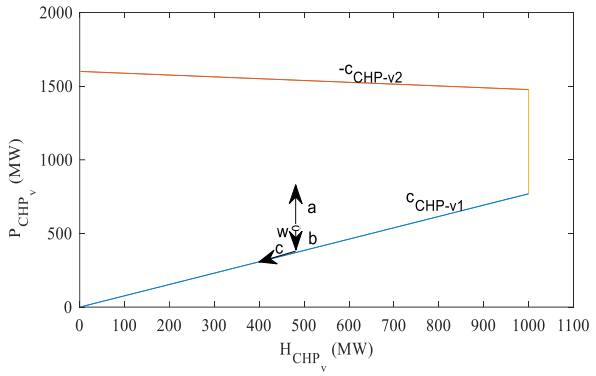

Fig. 2. Operation region and operating point variation of CHP with varied heat-to-electricity ratio.

- *Constraints of Electricity Network*

The AC power flow model is used to simulate the electric power network in IES, in which active and reactive power mismatches at bus i are calculated via (8)-(9). In (8)-(9), net active and reactive power injections $P_i^{\mathrm{SP}}(T)$ and $Q_i^{\mathrm{SP}}(T)$ at bus i are calculated as the difference between electric generation sources and loads, i.e. $P_i^{\mathrm{SP}}(T) = P_{\mathrm{G}i}(T) - P_{\mathrm{D}i}(T)$ and $Q_i^{\mathrm{SP}}(T) = Q_{\mathrm{G}i}(T) - Q_{\mathrm{D}i}(T)$.

$$\Delta P_i(T) = P_i^{\mathrm{SP}}(T) - \mathrm{Re}\left\{ U_i(T) \sum_{j \in N_i} \left(Y_{ij} U_j(T) \right)^* \right\} \tag{8}$$

$$\Delta Q_i(T) = Q_i^{\mathrm{SP}}(T) - \mathrm{Im}\left\{ U_i(T) \sum_{j \in N_i} \left(Y_{ij} U_j(T) \right)^* \right\} \tag{9}$$

Operation constraints include bus voltage limits (10) and transmission line loading capacities (11).

$$\underline{U_i} \le U_i(T) \le \overline{U_i} \tag{10}$$

$$-\overline{S_{ij}} \le S_{ij}(T) \le \overline{S_{ij}} \tag{11}$$

- *Constraints of Heating Network*

Heating network model is composed of a hydraulic and a thermal model. The hydraulic model describes the relationship between water pressures and mass flow rates. The continuity of flow is given as in (12). $\boldsymbol{A}$ is the node-pipe incidence matrix in which "0" describes a node is not connected to a pipe, while "+1" ("-1") indicates a node is the withdrawn (injection) node of the pipeline.

$$\boldsymbol{A} \cdot \boldsymbol{m}^{\mathrm{P}}(T) = \boldsymbol{m}^{\mathrm{N}}(T) \tag{12}$$

Heating network is associated with head losses, which refers to pressure changes due to pipe frictions. The loop pressure equation in (13) is used to describe that the summation of head losses around a closed loop is equal to zero. The pipe-loop incidence matrix $\boldsymbol{B}$ relates the pipes with corresponding loops, and $\boldsymbol{h}_{\mathrm{f}}(T)$ is the head loss vector of pipes at time T.

$$\boldsymbol{B} \cdot \boldsymbol{h}_{\mathrm{f}}(T) = 0 \tag{13}$$

Pipe hydraulic characteristics is given in (14), showing the relationship between mass flow rates and head losses along pipes, where resistance coefficient $\boldsymbol{R}$ can be referred to in [13].

$$\boldsymbol{h}_{\mathrm{f}}(T) = \boldsymbol{R} \cdot \boldsymbol{m}^{\mathrm{P}}(T) \cdot \left| \boldsymbol{m}^{\mathrm{P}}(T) \right| \tag{14}$$

Mass flow rate within heating pipeline is constrained by

$$-\overline{m^{\mathrm{P}}} \le m^{\mathrm{P}}(T) \le \overline{m^{\mathrm{P}}} \tag{15}$$

The thermal model describes the relationship between temperatures of water and the transmitted thermal energy. The heating power transferred to the load node is described as in (16).

$$\boldsymbol{\Phi}_{\mathrm{N}}(T) = CW \cdot \boldsymbol{m}^{\mathrm{N}}(T) \cdot \left[\boldsymbol{T}_{\mathrm{supp}}(T) - \boldsymbol{T}_{\mathrm{re}}(T) \right] \tag{16}$$

The temperature of water leaving a node with more than one incoming pipes is calculated as the weighted temperatures of all incoming flows (17).

$$\left(\sum m_{\mathrm{out}}^{\mathrm{P}}(T) \right) T_{\mathrm{out}}(T) = \sum m_{\mathrm{in}}^{\mathrm{P}}(T) T_{\mathrm{in}}(T) \tag{17}$$

- *Constraints of Natural Gas Network*

Similar to the electricity and heating networks, mass-flow balance at each gas node should be met. The nodal gas flow balance is modeled in (18), indicating the total gas flow injected into a node is equal to the withdrawn.

$$\boldsymbol{G} \cdot \boldsymbol{M}^{\mathrm{P}}(T) = \boldsymbol{M}^{\mathrm{N}}(T) \tag{18}$$

Gas flow through gas pipeline p with the two end nodes i and j is a nonlinear function of the nodal pressures π_i and π_j, as shown in (19). $sd_{ij}(T)$ is the sign function, and k_p is a constant of gas pipeline p.

$$M_p^{\mathrm{P}}(T) = k_p sd_{ij}(T) \sqrt{sd_{ij}(T)(\pi_i(T)^2 - \pi_j(T)^2)} \tag{19}$$

$$sd_{ij}(T) = \begin{cases} +1, \text{if } \pi_i(T) \ge \pi_j(T) \\ -1, \text{else} \end{cases} \tag{20}$$

Equation (19) can be reformulated as $M_p^{\mathrm{P}}(T) = \phi(\Delta\pi_p(T)^2)$ where $\Delta\pi_p(T)^2 = \pi_i(T)^2 - \pi_j(T)^2$ indicates the squared pipeline pressure drop and ϕ is a function denotation. Denoting $\Pi_i(T) = \pi_i(T)^2$ and $\Delta\Pi_p(T) = \Delta\pi_p(T)^2$, (21) can be derived.

$$\Delta\boldsymbol{\Pi}(T) = -\boldsymbol{G}^{\mathrm{T}} \boldsymbol{\Pi}(T) \tag{21}$$

Mass flow rate $M_p^{\mathrm{P}}(T)$ through gas pipeline p is also constrained by its capability limit as shown in (22).

$$-\overline{M_p^{\mathrm{P}}} \le M_p^{\mathrm{P}}(T) \le \overline{M_p^{\mathrm{P}}} \tag{22}$$

C. Solution Method

The inter-hour coordinated optimal scheduling problem is formulated via objective (1) and constraints (2)-(22), where constraints (8)-(9) and (19) are nonlinear. In an IES, with $\mathrm{NN_e}/\mathrm{NN_g}/\mathrm{NN_h}$ and $\mathrm{NB_e}/\mathrm{NB_g}/\mathrm{NB_h}$ electricity/gas/heating network nodes and branches, a set of continuous variables during the inter-hour scheduling horizon (including $\mathrm{NB_e}$ power flows, $\mathrm{NN_e}$-1 node angles and voltages, $\mathrm{NN_g}$ node gas pressures, $\mathrm{NB_g}$ gas mass flow rates, $\mathrm{NN_h}$ node temperatures, and $\mathrm{NB_h}$ water mass flow rates in supply and return heating networks) are to be solved by the inter-hour multi-energy

coupled scheduling.

The heuristic PSO algorithm integrated with the decomposed MEF calculation is developed, in order to effectively solve the proposed scheduling model with highly nonlinear MEF constraints. The procedure is described as follows:

Step 1) For a given scheduling horizon, hourly electric power outputs of CHPs with fixed heat-to-electricity ratio are chosen as particles to be optimized. Initialize positions and velocities of particles with respect to their boundaries.

Step 2) With the given electric power outputs of CHPs from the current particles in Step 1), their corresponding thermal power outputs are calculated via (2).

Step 3) For each hour, with the derived results in Steps 1) and 2) as well as the multi-energy demands from customers, a decomposition-based sequential MEF calculation is implemented:

(i) With heating power output of CHPs with fixed heat-to-electricity ratio, heating power flows through heating network and heating power of CHP with variable heat-to-electricity ratio are derived by the hydraulic-thermal model.

(ii) With electric power out of CHP with fixed heat-to-electricity ratio as input to the electricity network model, electric power flows through electricity lines and the electric power injection of CHP with variable heat-to-electricity ratio are determined.

(iii) Gas consumptions of CHPs are calculated via (3) and (7), which are then used as input to the gas network model to calculate gas flows of gas pipelines.

Step 4) Calculate fitness values of current particles. The fitness value is composed of the objective function (1) plus penalties on violations of constraints (5), (6), (10), (11), (15), and (22).

Step 5) Update the best individual position of each particle and the best global position among all particles.

Step 6) Update each particle's velocity ve_{d+1} and position x_{d+1} by $ve_{d+1} = iw \cdot ve_d + c_1 \cdot r_1 \cdot (gbest_d - x_d) + c_2 \cdot r_2 \cdot (pbest_d - x_d)$ and $x_{d+1} = x_d + ve_{d+1}$, where iw is inertia weight, x_d is particle's current position, $gbest_d$ is the best global position obtained in previous iterations, $pbest_d$ is the best position a particle has even had, r_1 and r_2 are uniformly distributed random numbers in [0,1], and c_1 and c_2 are adjustable parameters.

Step 7) If the maximum iteration $iter_{\max}$ is reached, go to Step 8); otherwise, go to Step 2).

Step 8) Output the particle with the minimum fitness value as the final solution.

The detailed procedure of decomposition-based sequential MEF calculation approach in Step 3) is further shown in Fig. 3. Electric power flow model, hydraulic-thermal model, and gas pipeline model are solved sequentially, so that the impact of CHPs on the coupled sub-networks can be accurately captured. In addition, Newton-Raphson algorithm is applied to solve the energy flow models of electricity, heating, and gas sub-networks in Step 3). The iterative procedure of Newton-Raphson method is given as follows:

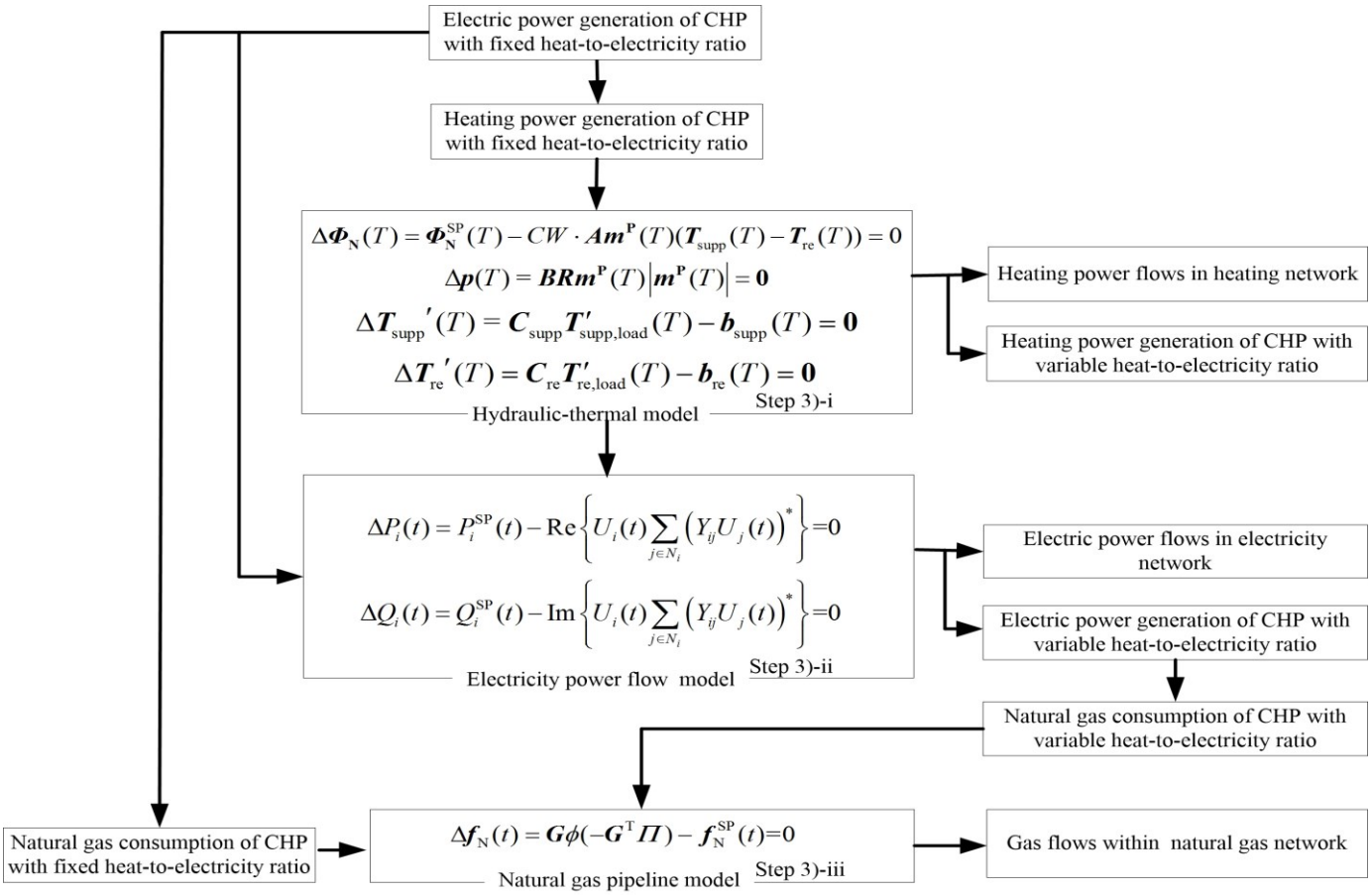

Fig. 3. Flowchart of decomposition-based approach for calculating MEF of integrated electrical-hydraulic-thermal-gas system.

$$\begin{cases}\Delta \boldsymbol{x}^{(k+1)} = (\boldsymbol{J}^{(k)})^{-1}\Delta \boldsymbol{F}^{(k)} \\ \boldsymbol{x}^{(k+1)} = \boldsymbol{x}^{(k)} - \Delta \boldsymbol{x}^{(k)}\end{cases} \tag{23}$$

where k is iteration index, $\boldsymbol{x}$ are state variables, $\boldsymbol{J}$ is Jacobian matrix, and $\Delta \boldsymbol{F}$ is the vector of total mismatches.

A key component of the Newton-Raphson algorithm is to calculate the Jacobi matrix. In electricity power flow model, Jacobi matrix is expressed as in (24), where $\Delta \boldsymbol{F}_{\mathrm{e}}(T) = \left[\Delta \boldsymbol{P}(T), \Delta \boldsymbol{Q}(T)\right]^{\mathrm{T}}$, $\boldsymbol{x}_{\mathrm{e}}(T) = \left[\boldsymbol{\theta}(T), \boldsymbol{U}(T)\right]^{\mathrm{T}}$. Equation (24) has been extensively studied in conventional electricity power flow analysis.

$$\boldsymbol{J}_{\mathrm{e}}(T) = \frac{\delta \Delta \boldsymbol{F}_{\mathrm{e}}(T)}{\delta \boldsymbol{x}_{\mathrm{e}}^{\mathrm{T}}(T)} \tag{24}$$

In the hydraulic-thermal system, the corresponding Jacobi matrix is denoted as in (25), where $\Delta \boldsymbol{F}_{\mathrm{h}}(T) = \left[(\Delta \boldsymbol{\Phi}_{\mathrm{N}}(T), \Delta p(T)), (\Delta \boldsymbol{T}'_{\mathrm{supp}}(T), \Delta \boldsymbol{T}'_{\mathrm{re}}(T))\right]^{\mathrm{T}}$ and $\boldsymbol{x}_{\mathrm{h}}(t) = \left[\boldsymbol{m}^{\mathrm{P}}(T), (\boldsymbol{T}'_{\mathrm{supp,load}}(T), \boldsymbol{T}'_{\mathrm{re,load}}(T))\right]^{\mathrm{T}}$. In turn, considering the detailed formulations in (12)-(17), Jacobian matrix $\boldsymbol{J}_{\mathrm{h}}(t)$ can be calculated as in (26).

$$\boldsymbol{J}_{\mathrm{h}}(T) = \frac{\delta \Delta \boldsymbol{F}_{\mathrm{h}}(T)}{\delta \boldsymbol{x}_{\mathrm{h}}^{\mathrm{T}}(T)} \tag{25}$$

$$\boldsymbol{J}_{\mathrm{h}}(T) = \begin{bmatrix} CW \cdot \boldsymbol{A} \cdot (\boldsymbol{T}_{\mathrm{supp}}(T) - \boldsymbol{T}_{\mathrm{out}}(T)) & Diag\left(CW \cdot \boldsymbol{A} \cdot \boldsymbol{m}^{\mathrm{P}}(T)\right) & 0 \\ 2\boldsymbol{BR}\left|\boldsymbol{m}^{\mathrm{P}}(T)\right| & 0 & 0 \\ 0 & \boldsymbol{C}_{\mathrm{supp}} & 0 \\ 0 & 0 & \boldsymbol{C}_{\mathrm{re}} \end{bmatrix} \tag{26}$$

For gas network, its Jacobian matrix is expressed as in (27), where $\Delta \boldsymbol{F}_{\mathrm{g}}(T) = \Delta \boldsymbol{M}^{\mathrm{N}}(T)$ and $\boldsymbol{x}_{\mathrm{g}}(T) = \boldsymbol{\Pi}(T)$. In turn, considering the detailed formulations in (18)-(22), $\boldsymbol{J}_{\mathrm{g}}(T)$ can be represented as in (28), where $\boldsymbol{D}(T) = Diag\left(\frac{1}{2}\frac{M_p^{\mathrm{P}}(T)}{\Delta \Pi_p(T)}\right)$ for each pipeline p.

$$\boldsymbol{J}_{\mathrm{g}}(T) = \frac{\delta \Delta \boldsymbol{F}_{\mathrm{g}}(T)}{\delta \boldsymbol{x}_{\mathrm{g}}^{\mathrm{T}}(T)} \tag{27}$$

$$\boldsymbol{J}_{\mathrm{g}}(T) = = -\boldsymbol{G}\boldsymbol{D}(T)\boldsymbol{G}^{\mathrm{T}} \tag{28}$$

With the above three Jacobi matrices, the steady-state MEF of the IES can be effectively calculated.

IV. Intra-Hour Dispatching to Mitigate Uncertainties with Gas Linepack

In an islanded IES without the support of the main grid, because of limited resource availability to compensate uncertain power outputs of RESs, maintaining electricity supply/demand balance is even more imperative than in the grid-connected IES. As it takes considerable time to deliver gas from a source node to its intended destination, it is physically infeasible to adjust gas flow rate at source node for supporting CHPs to mitigate instantaneous fluctuations of RESs. On the other hand, natural gas can be stored in the pipeline for the use in short-term operations. Indeed, the linepack within a pipeline, defined as the amount of stored gas, is proportional to the average pressure. Therefore, increasing average pressure of pipelines could increase the linepack. However, in most existing multi-energy scheduling research, pressures of gas source nodes are usually pre-specified, which could be further optimized to provide better linepack capacities for mitigating RES uncertainties.

A. Adjustment of CHP Operating Point

When mitigating the fluctuations and intermittencies of RES in intra-hour dispatching, in order to reduce the influence on the heating supply/demand balance, the operation adjustment is only implemented on the CHP unit with variable heat-to-electricity ratio. For this type of CHPs, the relationship between heating and electrical power outputs is depicted in Fig. 2. The adjustment strategy is illustrated as follows. Assuming that the CHP unit at gas node *i* operates at point *w* and the corresponding mass flow rate of electricity generation gas consumption is M_i^{N}, which is determined by inter-hour scheduling, in the intra-hour scheduling, if RES outputs decrease, the operating point of CHP moves along the direction of Line *a*; Otherwise, if RES outputs increase, its operating point changes along the direction of Line *b*, and then follows the direction of Line *c* after it reaches the lower boundary.

B. Determination of Extreme Scenarios of RES Outputs

During the intra-hour period, dynamic scenarios generation method proposed in [22] are used, which represent not only the marginal distribution of possible RES generation outputs at each sampling time instant, but also the joint distribution among multiple outputs at different time instants. Moreover, the number of scenarios SN_{RES} is determined when the Kantorovich distance between the generated scenarios and historical data becomes stable with the increase in the number of scenarios.

Inter-hour scheduling results aim at achieving the gas supply/demand balance with respect to the forecasted RES power outputs $P_{\mathrm{P\_RES}}$. However, the difference between actual and predicted RES power outputs during the intra-hour period could induce supply/demand unbalance. In the intra-hour scheduling, with the time-resolution of RES outputs of t_{R} minutes, RES power output scenario s can be denoted as $P_{\mathrm{S\_RES}}^{s} = \left[P_{\mathrm{S\_RES}}^{s,1}, \cdots \right.$ $\left.\right|$ where $RN = 60/t_{\mathrm{R}}$. For each scenario s, according to the difference between $P_{\mathrm{P\_RES}}$ and $P_{\mathrm{S\_RES}}^{s}$, the adjustment of CHP operating points can be determined and then its gas consumption $\left[\underbrace{\cdots}_{\cdots,\mathrm{R}} \quad \underbrace{\cdots}_{\cdots,\mathrm{R}}\right]$ during the intra-hour dispatching period can be obtained. Consequently, during the intra-hour period, the change of total gas volume stored in the entire gas pipelines in scenario s can be derived as in (29).

$$\Delta LinePack_{s,RT} = \sum_{j=1}^{RT}(M_i^{\mathrm{N}} - M'_{i,j,s}) \cdot t_{\mathrm{R}} \cdot 60, \quad s = 1, \cdots \quad \cdots \tag{29}$$

where the natural gas mass flow rates M_i^{N} and $M'_{i,j,s}$ are measured in kg/s.

Finally, among all scenarios SN_{RES}, two extreme scenarios $\overline{s}$ and $\underline{s}$ with the largest increase and decrease of $\Delta LinePack_{s,RT}$ can be identified.

C. Dynamic Transmission Model in Gas Pipeline

In intra-hour scheduling model, due to the non-ignorable natural gas travelling time, the steady-state model of gas network is unsuitable and consequently the dynamic transmission model is applied.

Specifically, for a gas pipeline with two end nodes i and j, the partial differential equation (30) expresses the mass conservation.

$$\pi'_{j,t+1}+\pi'_{i,t+1}-\pi'_{j,t}-\pi'_{i,t}+\frac{\Delta t\cdot c^2}{L_{ij}S_{ij}}\left[M'_{j,t+1}-M'_{i,t+1}+M'_{j,t}-M'_{i,t}\right]=0 \quad (30)$$

In addition, for each pipeline, the momentum transport in the continuum of natural gas is described as in (31). Parameter $\overline{f}_{ij,t}=\dfrac{f_{i,t}+f_{j,t}}{2}$ is the average gas flow rate in m/s at time t, and $c^2=RTZ$ with gas constant R=500, temperature T=273 K, and compressibility factor Z=0.9.

$$\begin{aligned}&\frac{c^2}{S_{ij}}\left(M'_{j,t+1}+M'_{i,t+1}-M'_{j,t}-M'_{i,t}\right)+\frac{\Delta t}{L_{ij}}\left(\pi'_{j,t+1}+\pi'_{i,t+1}-\pi'_{j,t}-\pi'_{i,t}\right)\\&\qquad+\frac{c^2\lambda\overline{f}_{ij,t}\Delta t}{4d_{ij}S_{ij}}\left(M'_{j,t+1}+M'_{i,t+1}+M'_{j,t}+M'_{i,t}\right)=0\end{aligned} \quad (31)$$

Furthermore, at an intersection where nodes i, i+1, i+2, … are connected, there should be a consensus gas pressure and a balanced mass flow rate as shown in (32)-(33).

$$\pi'_{i,t}=\pi'_{i+1,t}=\pi'_{i+2,t}\cdots \quad (32)$$

$$M'_{i,t}+M'_{i+1,t}+M'_{i+2,t}\cdots \quad (33)$$

Mass flow rate at source node and node of CHP with fixed heat-to-electricity ratio should be equal to the scheduled values determined in the inter-hour scheduling, i.e. $M'_{i,t}=M_i^{\mathrm{N}}(T)$, $i\in N_{\mathrm{gs}}, N_{\mathrm{CHP\_c}}, t\in T$.

Mass flow rates at non-generation gas load nodes $M'_{i,t}, i\in N_{\mathrm{L}}$ are already known, and that at CHP node with variable heat-to-electricity ratio for scenario s is

$$\left[M' \underbrace{\qquad\qquad}_{60\cdot t_{\mathrm{R}}} \quad \underbrace{\qquad\qquad}_{60\cdot t_{\mathrm{R}}}\right],\ i\in N_{\mathrm{CHP\_v}}.$$

For gas node i, constraints (34)-(35) should be satisfied.

$$M'_{i,t}=f_{i,t}\rho_{i,t}A_{ij} \quad (34)$$

$$\rho_{i,t}=\pi'_{i,t}/c^2 \quad (35)$$

Equations (30)-(35) constitute a linear programming (LP) problem, in which the mass flow rates and pressures at all nodes at time t+1 can be derived according to those at time t. In the simulation, in order to improve the accuracy of partial differential approximation based dynamic model, the iteration time step is set as one second.

Moreover, gas pressure bounds of load nodes should be imposed as in (36).

$$\underline{\pi}_i\le\pi'_{i,t}\le\overline{\pi}_i, i\in N_{\mathrm{Non\_gen}}, N_{\mathrm{CHP\_v}}, N_{\mathrm{CHP\_c}} \quad (36)$$

The pressures and mass flow rates at the two ending nodes of a pipeline are different from each other; Moreover, their values at time t may be different from those at time t+1 due to dynamic gas transmissions. For a pipeline with two end nodes i and j, there are 8 continuous variables $\pi'_{i,t}$, $M'_{i,t}$, $\pi'_{j,t}$, $M'_{j,t}$, $\pi'_{i,t+1}$, $M'_{i,t+1}$, $\pi'_{j,t+1}$, and $M'_{j,t+1}$. Eqs. (30)-(35), along with the known mass flow rates at source node, electricity generation and non-generation load nodes at time t, constitute 8*$\mathrm{NB_g}$ equations to determine the values of these variables.

D. Solution Procedure of Intra-hour Dispatching

The objective of intra-hour dispatching strategy is to determine a robust pressure region for $\pi'_{i,t}\left(i\in N_{\mathrm{gs}}\right)$ at gas source node when the intra-hour dispatching starts at time t=1, with which all gas load nodes can work within the required pressure range during the entire intra-hour time period under the two extreme RESs scenarios.

The procedure of intra-hour dispatching is illustrated:

Step 1) Set initial pressure range of source node according to the inter-hour scheduled mass flow rates and the required pressure ranges at load nodes, and the change step of source node pressure considering the usual valve operation;

Step 2) For each candidate pressure at source node and each extreme RES scenario, solve the LP problem (30)-(35) by Cplex iteratively to derive gas pressures and mass flow rates during the entire intra-hour time period, i.e. the derived pressures and mass flow rates values from the LP problem at time t is used as inputs to the LP problem at time $t+1$;

Step 3) For the two extreme scenarios, considering the upper and lower bounds for gas pressures at load nodes, determine their corresponding source node pressure ranges and the intersection of them describe the robust pressure range of the source node.

V. Simulation Results

In this work, an islanded IES shown in Fig. 4 is used to assess and validate the proposed optimal two-timescale multi-energy coordinated scheduling approach. The IES is composed of an 8-bus electricity sub-system, a 9-node heating sub-system, and an 8-node natural gas sub-system. In Fig. 4, loads are indicated as hollow circle nodes. Hourly electricity, heating, and non-generation demands in inter-hour scheduling period are known. In inter-hour scheduling, the pressure at gas source node is set as 0.705 Mpa, and the supply temperature at source node and the return temperature at load node are set as 100 °C and 50 °C, respectively. Two coupling energy components, the gas turbine CHP1 and the extraction turbine CHP2, are included in the system, and a wind turbine is located at node EB6. Data of system components and parameters of electrical, heating, and gas sub-networks are detailed in Appendix. As for the PSO algorithm, the parameters are chosen as $c_1=c_2=1.49$, $iw=0.75$, and $iter_{\max}=50$.

A. Inter-Hour Scheduling

Multi-energy supply and demand balance is the fundamental requirement for the IES operation. As shown in Figs. 5-7, inter-hour scheduling results on electricity, heating, and gas can achieve multi-energy supply/demand balances. Mass flow rates in heating and gas networks are depicted in Figs. 8 and 9. Real power flows through electricity lines and bus voltage magnitudes are given in Figs. 10 and 11. Constraints on energy flows of electricity,

heating and gas are all satisfied. In the islanded mode, the gas turbine CHP1 has a higher efficiency while the extraction turbine CHP2 is used for system source-load balance. Thus, as shown in Figs. 5 and 6, outputs of CHP1 are higher than those of CHP2.

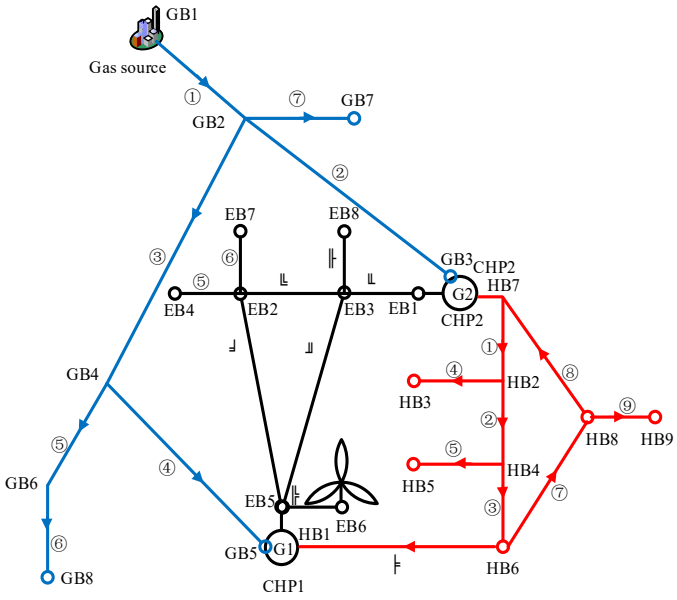

Fig. 4. Diagram of an integrated energy test system.

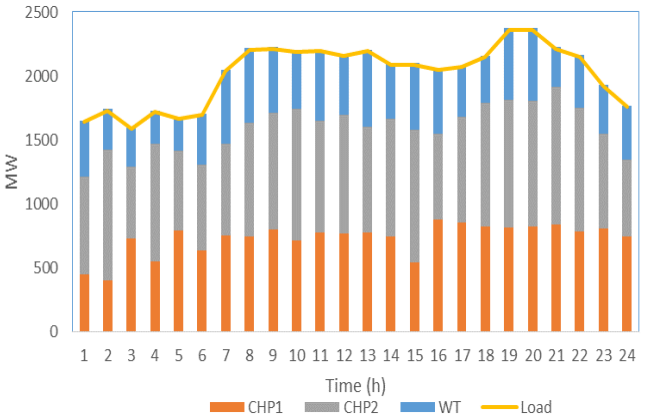

Fig. 5. Supply/demand balance of electricity energy.

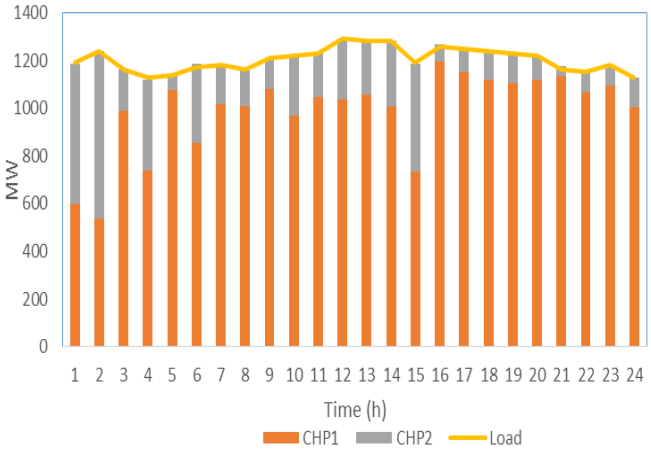

Fig. 6. Supply/demand balance of heating energy.

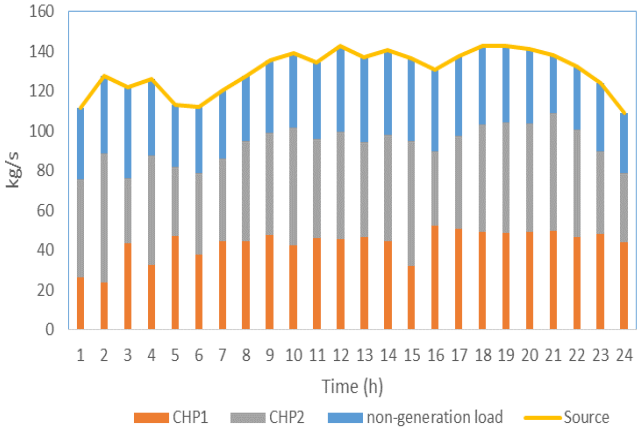

Fig. 7. Supply/demand balance of natural gas.

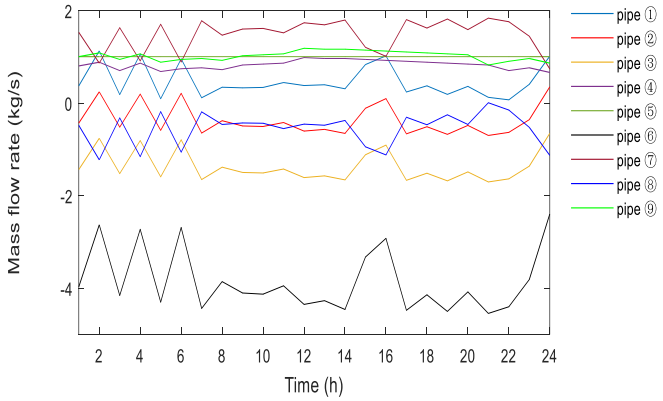

Fig. 8. Mass flow rate through pipelines in heating network.

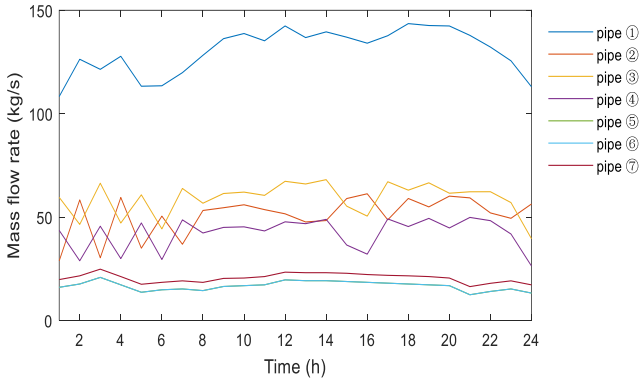

Fig. 9. Mass flow rate through pipelines in gas network.

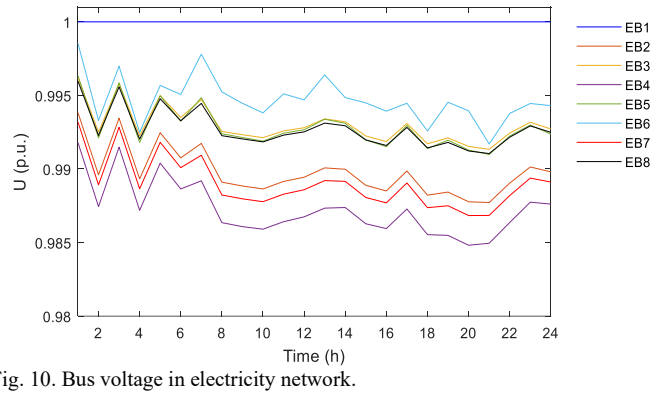

Fig. 10. Bus voltage in electricity network.

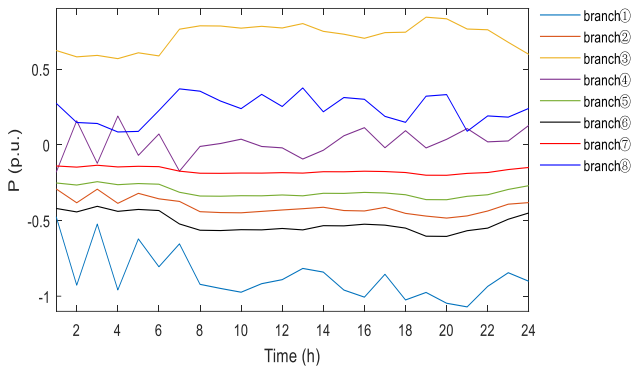

Fig. 11. Real power flows through electricity lines.

B. Intra-Hour Dispatching

The first hour is used as an example to illustrate how to derive the robust range of gas pressure at source node through the intra-hour dispatching. By measuring the change of Kantorovich distance between the dynamic scenarios of wind turbine power outputs and its historical data against different numbers of scenarios, SN_{RES} is chosen as 100. For each scenario s in SN_{RES}, the operating point variation of CHP2 can be determined and its gas consumption during the intra-hour period can be obtained. Among the 100 scenarios, two extreme scenarios are identified respectively with the largest and the smallest $\Delta LinePack_{s,RT}$. Gas consumptions of CHP2 in the two extreme scenarios and other three randomly selected scenarios, as well as its inter-hour scheduled value are depicted in Fig. 12. The corresponding pipeline linepack variations of these five scenarios are given in Fig. 13. As shown in Fig. 12, gas consumption of CHP2 in scenario 4 keeps higher than its inter-hour scheduled value almost in the entire intra-hour period, and consequently its corresponding variation of linepack decreases greatly. The situation in scenario 5 is opposite. Scenarios 4 and 5 are chosen as the extreme scenarios to determine the robust range of gas pressure at source node.

The lower and upper pressure limits at non-generation and CHPs nodes are chosen as $\underline{\pi}_i$=0.45 MPa and $\overline{\pi}_i$=0.65 MPa, and the pressure adjustment step at source node is set as 0.2 KPa. The pressure ranges at source node for the two extreme scenarios are obtained as $\pi'_{i,1} \in [0.6748, 0.7354]$ MPa and $\pi'_{i,1} \in [0.6720, 0.7472]$ MPa, respectively. Consequently, the robust pressure range at source node is $\pi'_{i,1} \in [0.6748, 0.7354]$ MPa.

With the scheduled gas source pressure $\pi'_{i,1}$=0.6748 MPa, the mass flow rates and pressures at all gas nodes in scenario 4 are depicted in Figs. 14 and 15. As shown in Fig. 14, in the extreme scenario 4 with a higher CHP2 gas consumption than forecasting, pressure at GB5 still stays higher than its lower limit during the entire hour when the lower bound $\pi'_{i,1}$=0.6748 of pressure region is implemented on gas source node. In the other extreme scenario 5 where the real wind power generation is larger than its forecasting during most of the scheduled hour, with the upper bound $\pi'_{i,1}$=0.7354 MPa of the scheduled range, the mass flow rates and pressures of all gas nodes in scenario 5 are depicted in Figs. 16 and 17, and the pressure at GB5 can maintain within the operation secure constraint during the entire hour.

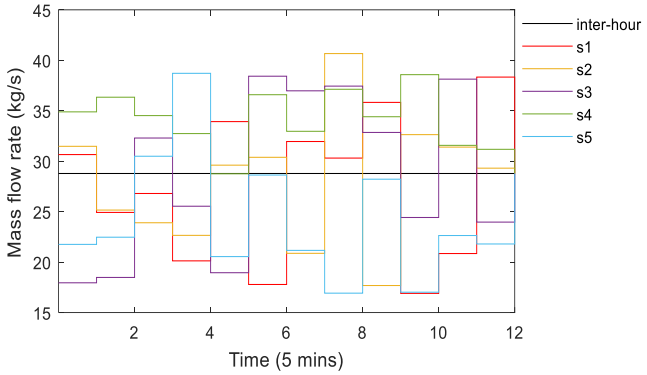

Fig. 12. Gas consumptions of CHP2 in wind power scenarios.

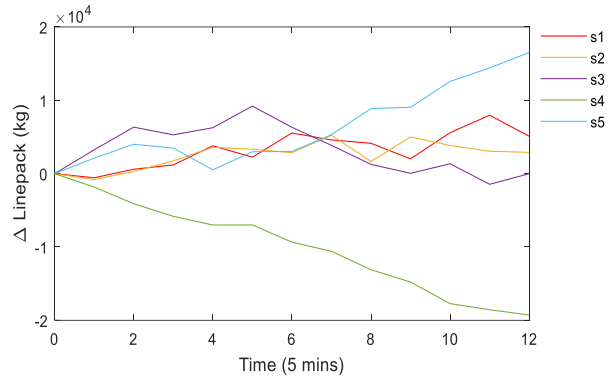

Fig. 13. Linepack variation of gas pipeline in wind power scenarios.

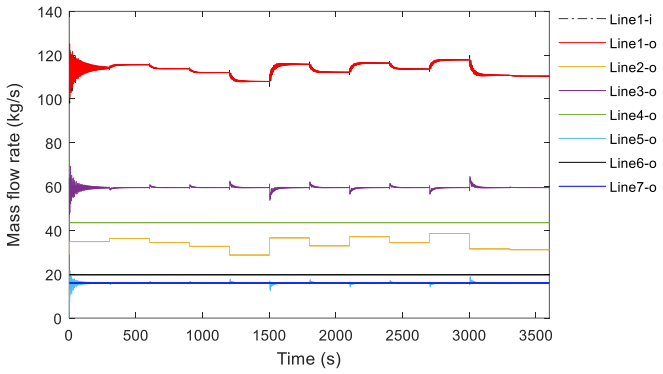

Fig. 14. Mass flow rate at gas nodes in scenario 4 with $\pi'_{i,1}$=0.6748 MPa at node GB1.

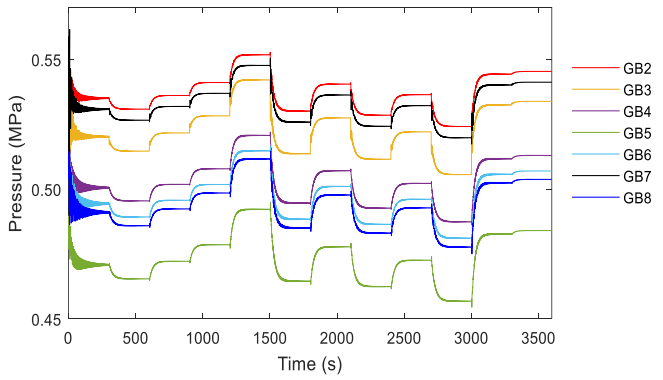

Fig. 15. Gas node pressure in scenario 4 with $\pi'_{i,1}$=0.6748 MPa at node GB1.

With a certain gas source pressure $\pi'_{i,1}$=0.6905 MPa and a randomly generated wind power scenario, the mass flow rates and pressures in gas pipelines are depicted in Figs. 18 and 19, validating the effectiveness of the proposed method against RESs uncertainties by utilizing the flexibility offered

via the storage characteristics of gas network.

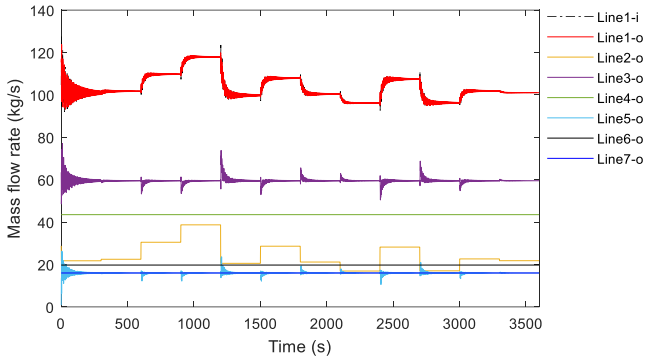

Fig. 16. Mass flow rate at gas nodes in scenario 5 with $\pi'_{i,1}$ =0. 7354 MPa at node GB1 (-o: outlet, -i: inlet).

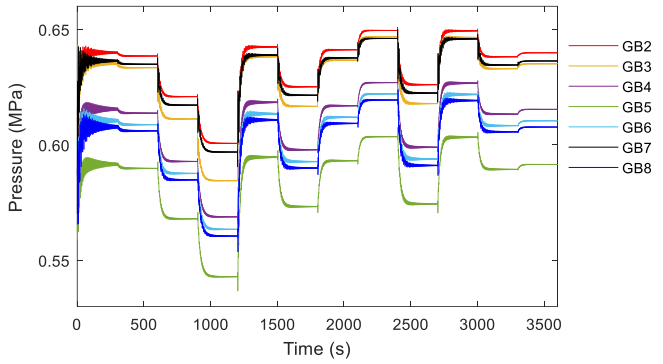

Fig. 17. Gas node pressure in scenario 5 with $\pi'_{i,1}$ =0. 7354 MPa at node GB1.

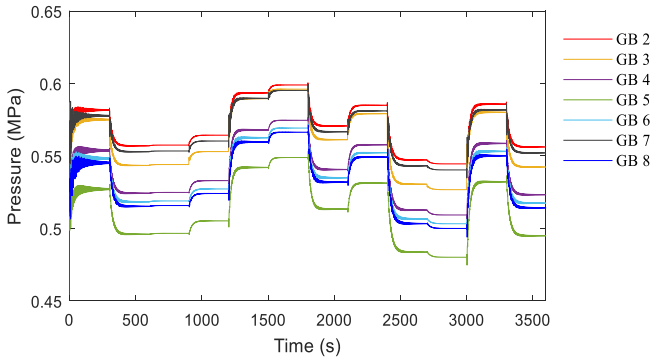

Fig. 18. Gas node pressure in a random wind power generation scenario with $\pi'_{i,1}$ =0. 6905 MPa at node GB1.

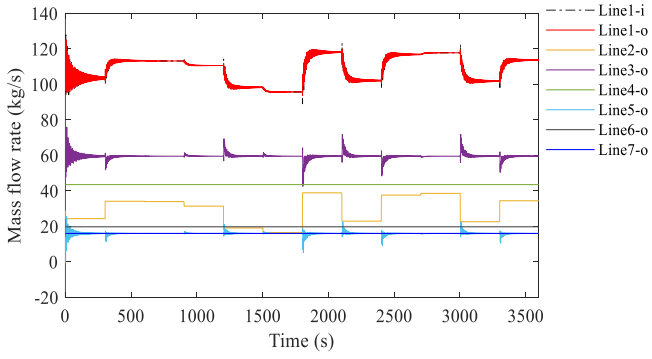

Fig. 19. Mass flow rate at gas nodes in a random wind power generation scenario with $\pi'_{i,1}$ =0. 6905 MPa at node GB1 (-o: outlet, -i: inlet).

C. Comparison between Natural Gas Steady-State Model and Dynamic Model based Intra-Hour Dispatching

When the gas steady-state model is employed in intra-hour dispatching, the robust pressure range at gas source node considering the above two extreme scenarios can be obtained as $\pi'_{i,1} \in [0.6707, 0.7380]$ MPa , which is obviously wider than the scheduled result derived from th egas dynamic model based intra-hour dispatching. When the gas source pressure is scheduled to be the two bounds of the robust range $\pi'_{i,1} \in [0.6707, 0.7380]$ MPa , the nodes pressures within gas network considering gas dynamics are represented in Figs. 20 and 21. It can be observed that, when the upper bound $\pi'_{i,1}$ =0.7380 MPa of gas source pressure encounters the worst scenario 5 or the lower bound $\pi'_{i,1}$ =0.6707 MPa of gas source pressure encounters the worst scenario 4, gas pressure at the CHP node will be outside the operation security constraint. It can be inferred that, the steady-state natural gas flow model, which neglects the built-in storage capabilities of pipelines and the slower travelling of gas flows, may result in non-optimal results in intra-hour dispatching.

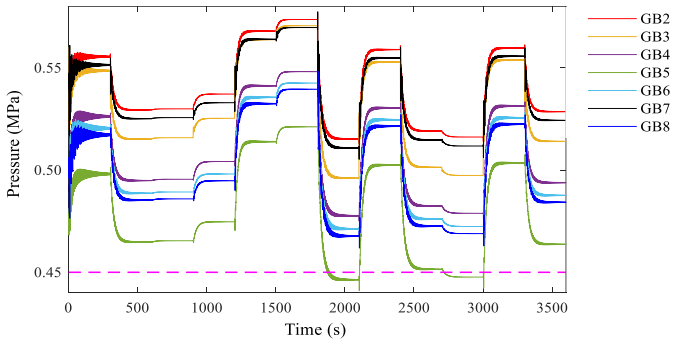

Fig. 20. Gas node pressure in scenario 4 with $\pi'_{i,1}$ =0. 6707 MPa at node GB1.

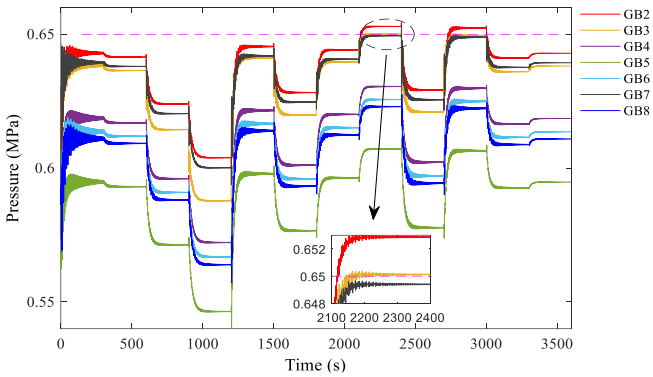

Fig. 21. Gas node pressure in scenario 4 with $\pi'_{i,1}$ =0. 7380 MPa at node GB1.

D. Discussion on the Ability in Capturing Dynamic Effects

With the gas source node pressure $\pi'_{i,1}$=0.6748 MPa and the mass flow rate fluctuation occurring once every 5 minutes at the outlet of Line 2, the node pressures and pipeline mass flow rates derived by steady-state and dynamical gas models are respectively drawn in Figs. 22 and 23.

In Fig. 22, the lines labeled as Line1 and Line3 represent the steady-state model derived mass flow rates through Lines 1 and 3, since in the steady-state model there is no difference between the flow rates at the outlet and inlet of a pipeline. As shown in Fig. 22, compared with the natural gas steady-state model, the dynamic model describes more details of the transient process. Although the stable values of mass flow

rates after the transient process is equal to the values derived by the steady-state model, fluctuations of the mass flow rate during dynamic process do exist. Moreover, there are discrepancies between the nodes pressures calculated by the steady-state and dynamic models. Indeed, Fig. 22 shows that the pressure errors of steady-state model becomes larger as the node goes far away from the gas source. Consequently, the dynamic model is more accurate than the steady-state model in capturing transition effects of gas transmission.

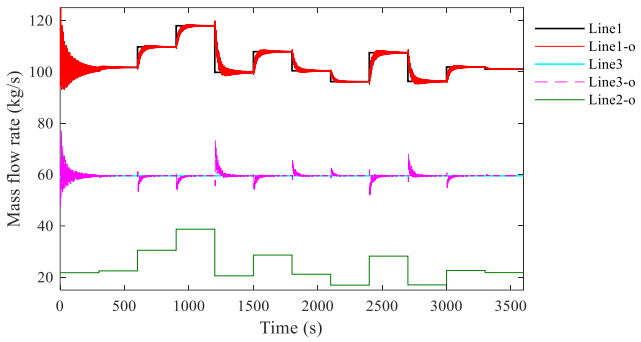

Fig. 22. Comparison of mass flow rate between steady-state model and dynamic model (-o: outlet, -i: inlet).

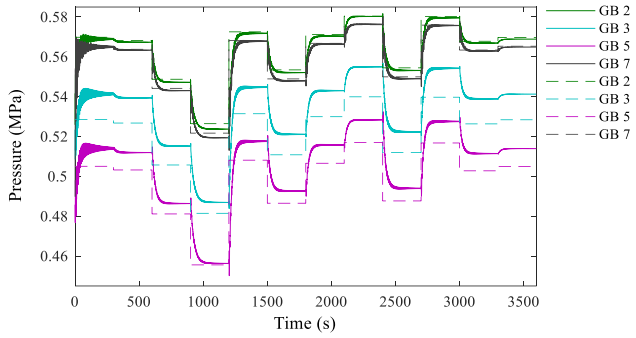

Fig. 23. Comparison of node pressure between steady-state model and dynamic model.

VI. Conclusions

In order to achieve the coordinated optimal scheduling of multi-energy with distinct response time and improve the robustness of IES against RES uncertainties, a combined inter-hour and intra-hour multi-energy scheduling approach for an electrical-hydraulic-thermal-gas IES operated in islanded mode is proposed. The response time differences among energy subsystems are considered in the coupled two-timescale optimization by using steady-state and dynamic models respectively to capture the characteristics representing in different timescales. Two types of CHPs with complimentary properties are scheduled to enable the coordination in meeting the electricity and thermal energy demands and achieving operational economics as well, especially for the islanded IES where the strict balance between energy supply and demand has to be handled by itself. Robust pressure range at source node is optimized to ensure that the fluctuation of CHP gas consumption can be satisfied by the gas linepack existing in the transportation infrastructures when mitigating the RESs uncertainties. The necessity of considering gas transmission dynamics in intra-hour dispatching is demonstrated by comparing the proposed approach with natural gas steady-state model based intra-hour. Simulation results corroborate the effectiveness of the proposed approach, which could pave the way of developing an integrated optimization solution framework of IES.

References

[1] M. Omalley and B. Kroposki, "Energy comes together: the integration of all systems," IEEE Power Energy Mag., vol. 11, no. 5, pp. 18-23, Sep. 2013.

[2] P. Mancarella, "MES (multi-energy systems): An overview of concepts and evaluation models," Energy, vol. 65, pp. 1-17, Feb. 2014.

[3] C. Wang, W. Wei, J. Wang, L. Bai, Y. Liang and T. Bi, "Convex optimization based distributed optimal gas-power flow calculation," *IEEE Trans. Sustain. Energy*, vol. 9, no. 3, pp. 1145-1156, Jul. 2018.

[4] Y. He, M. Shahidehpour, Z. Li, C. Guo and B. Zhu, "Robust constrained operation of integrated electricity-natural gas system considering distributed natural gas storage," *IEEE Trans. Sustain. Energy*, vol. 9, no. 3, pp. 1061-1071, Jul. 2018.

[5] L. Bai, F. Li, H. Cui, T. Jiang, H. Sun and J. Zhu, "Interval optimization based operating strategy for gas-electricity integrated energy systems considering demand response and wind uncertainty," *Appl. Energy*, vol. 167, pp. 270-279, Apr. 2016.

[6] A. Alabdulwahab, A. Abusorrah, X. Zhang and M. Shahidehpour, "Coordination of interdependent natural gas and electricity infrastructures for firming the variability of wind energy in stochastic day-ahead scheduling," *IEEE Trans. Sustain. Energy*, vol. 6, no. 2, Apr. 2015.

[7] X. D. Xu, X. L. Jin, H. J. Jia, X. D. Yu and K. Li, "Hierarchical management for integrated community energy systems," *Appl. Energy*, vol. 160, pp. 231-243, Dec. 2015.

[8] Z. Pan, Q. Guo and H. Sun, "Interactions of district electricity and heating systems considering time-scale characteristics based on quasi-steady multi-energy flow," *Appl. Energy*, vol. 167, pp. 230-243, Apr. 2016,

[9] Z. Qiao, Q. Guo, H. Sun, Z. Pan, Y. Liu and W. Xiong, "An interval gas flow analysis in natural gas and electricity coupled networks considering the uncertainty of wind power," *Appl. Energy*, vol. 201, pp. 343-353, Sep. 2017.

[10] Z. Li, W. Wu, J. Wang, B. Zhang and T. Zheng, "Transmission-constrained unit commitment considering combined electricity and district heating networks," *IEEE Trans. Sustain. Energy*, vol. 9, no. 3, pp. 1145-1156, Jul. 2018.

[11] Z. Li, W. Wu, M. Shahidehpour, J. Wang, B. Zhang, "Combined heat and power dispatch considering pipeline energy storage of district heating network," *IEEE Trans. Sustain. Energy*, vol. 7, no. 1, pp. 12-22, Jan. 2016.

[12] X. Liu, J. Wu, N. Jenkins and A. Bagdanavicius, "Combined analysis of electricity and heat networks," *Appl. Energy*, vol. 162, pp. 1238-1250, Jan. 2016.

[13] X. D. Xu, X. L. Jin, H. J. Jia, X. D. Yu and K. Li, "Hierarchical management for integrated community energy systems," *Appl. Energy*, vol. 160, pp. 231-243, Dec. 2015.

[14] C. Shao, Y. Ding, J. Wang and Y. Song, "Modeling and integration of flexible demand in heat and electricity integrated energy system," *IEEE Trans. Sustain. Energy*, vol. 9, no. 1, Jan. 2018.

[15] Q. Zeng, J. Fang, J. Li and Z. Chen, "Steady-state analysis of the integrated natural gas and electric power system with bi-directional energy conversion," *Appl. Energy*, vol. 184, pp. 1483-1492, Dec. 2016.

[16] G. Li, R. Zhang, T. Jiang, H. Chen, L. Bai and X. Li, "Security-constrained bi-level economic dispatch model for integrated natural gas and electricity systems considering wind power and power-to-gas process," *Appl. Energy*, vol. 194, pp. 696-704, May. 2017.

[17] A. Alabdulwahab, A. Abusorrah, X. Zhang and M. Shahidehpour, "Stochastic security-constrained scheduling of coordinated electricity and natural gas infrastructure," *IEEE Syst. Journal*, vol. 11, no. 3, pp. 1674-1683, Sep. 2017.

[18] X. Jin, Y. Mu, H. Jia, J. Wu, X. Xu and X Yu, "Optimal day-ahead scheduling of integrated urban energy systems," *Appl. Energy*, vol. 180, pp. 1-13, Oct. 2016.

[19] C. Liu, M. Shahidehpour and J. Wang, "Coordinated scheduling of electricity and natural gas infrastructures with a transient model for natural gas flow," *Chaos.*, vol. 21, Jun. 2011.

[20] S. Clegg and P. Mancarella, "Integrated electrical and gas network flexibility assessment in low-carbon multi-energy systems," *IEEE Trans. Sustain. Energy*, vol. 7, no. 2, pp. 718-731, Apr. 2016.

[21] C. M. Correa-Posada and P. Sanchez-Martin, "Integrated power and natural gas model for energy adequacy in short-term operation," *IEEE Trans. Power Syst.*, vol. 30, no. 6, pp. 3347-3355, Nov. 2015.

[22] Z. Bao, W. Qiu, L. Wu, F. Zhai, W. Xu, B. Li and Z. Li, "Optimal multi-timescale demand side scheduling considering dynamic scenarios of electricity demand," *IEEE Trans. Smart Grid*, to appear, DOI: 10.1109/TSG.2018.2797893.

Appendix

Table A1. Parameters of CHP1

$c_{\mathrm{CHP\_f}}$	$a_{\mathrm{CHP\_f}}$	$\overline{P_{\mathrm{CHP\_f}}}$ (MW)
1.357	2.6433	1000

Table A2. Parameters of CHP2

$c_{\mathrm{CHP\_v1}}$	$c_{\mathrm{CHP\_v2}}$	$a_{\mathrm{CHP\_v}}$	$b_{\mathrm{CHP\_v}}$	$g_{\mathrm{CHP\_v}}$	$\overline{P_{\mathrm{CHP\_v}}}$ (MW)	$\overline{H_{\mathrm{CHP\_v}}}$ (MW)
1.3	1/8.1	0.59	2.4	3.59	1600	1000

Table A3. Constraints for electricity, heating and gas network

$\underline{U}$ (p.u.)	$\overline{U}$ (p.u.)	$\overline{S}$ (p.u.)	$\overline{m^{\mathrm{P}}}$ (kg/s)	$\overline{M^{\mathrm{P}}}$ (kg/s)
0.95	1.05	1.1	5	200

Table A4. Parameters of electricity network

Branch no	Start bus	End bus	R+j·X
1	1	3	0.008+ j·0.003
2	3	2	0.008+ j·0.003
3	2	5	0.004 + j·0.0025
4	5	3	0.001 + j·0.0035
5	2	4	0.008+ j·0.0015
6	2	7	0.0015 + j·0.0035
7	3	8	0.0015 + j·0.0035
8	5	6	0.008 + j·0.0035

Table A5. Pipeline parameters of gas network

Length L (m)	Diameter d (m)	Friction factor λ
500	0.6	0.01

Table A6. Decision variables bounds

Variables	Upper bound	Lower bound
U (p.u.)	1.05	0.95
θ (rad)	0.5	-0.5
P (p.u.)	1	-1
M (Kg/s)	6	-6
$\boldsymbol{T}_{\mathrm{supp}}$ (℃)	100	50
$\boldsymbol{T}_{\mathrm{re}}$ (℃)	50	0
π (MPa)	0.65	0.45
M (Kg/s)	200	-200